IAC-21-A6.5.9

Rendezvous and Proximity Operations Design of an Active Debris Removal Service to a Large Constellation Fleet

Giacomo Borelli [a]*, Gabriella Gaias[a], Camilla Colombo[a], Lorenzo Vallini[b]

[a] *Department of Aerospace Science and Technology, Politecnico di Milano, Via La Masa 34, 20156, Milan, Italy.*
[b] *D-Orbit SpA, Viale Risorgimento, 57 22073 Fino Mornasco, Como, Italy.*
* Corresponding Author: giacomo.borelli@polimi.it

Abstract

Large constellations' deployment in low Earth orbit will drastically change the space environment and economy in the upcoming decades. The sustainability of the orbital environment in the long term needs to be accounted when implementing the large constellations projects. In fact, failures among the large constellations' assets can critically endanger the congested orbital region increasing the risk of collisions. Particularly for the higher altitude constellations, where the atmospheric drag will not contribute to the natural deorbit of the debris satellites. In this paper, an Active Debris Removal (ADR) service targeted to large constellations is developed, where a servicer is employed to safely deorbit the failed assets by performing a rigid capture. The content of this work comprehends the phase A design of the proximity operations to the uncooperative and non-collaborative failed constellations satellites. The design of the proximity concept of operations has been driven by the repeatability of the service, safety, and autonomy of operations. The initial trade-off on the rendezvous approach Guidance Navigation and Control (GNC) is presented, where solutions to enhance the convergence of the angles-only navigation are employed. Additionally, the design of the proximity phases of inspection and rigid control capture preparation through contactless detumbling of the debris are described, in terms of the approach strategy and feasibility. Finally, the delta-v budget is provided. The proximity operations design presented in this paper was the base of the phase A design of the active debris removal service performed within the ESA/OneWeb Sunrise programme.

Keywords: Active debris removal, Large constellation, Proximity operations, GNC

Nomenclature

$a\delta\boldsymbol{\alpha}$	ROE vector, m
$\Delta a\delta\boldsymbol{\alpha}$	ROE impulsive jump, m
Φ	State transition matrix of the relative motion in ROE
B	Impulsive control input matrix of relative motion in ROE
$\delta\boldsymbol{v}$	Impulsive delta-v vector, m/s
$\delta\boldsymbol{x}$	Relative cartesian state in RTN, m and m/s
$\boldsymbol{X}$	Guidance ROE jumps vector, m
J	Guidance cost function, [m^2]
w	Observability guidance weight
u	Argument of latitude, rad or deg
$\delta\hat{\boldsymbol{\alpha}}$	Estimated ROE state, m
$\boldsymbol{\omega_0}$	Initial target angular rate vector in its body frame, rad/s or deg/s
$\boldsymbol{F_{imp}}$	Impingement thruster, N
θ_0	Plume half cone angle, rad or deg

Acronyms/Abbreviations

ADR	Active Debris Removal
AE	Approach Ellipsoid
ConOps	Concept of Operations
EKF	Extended Kalman Filter
FOV	Field Of View
GNC	Guidance Navigation and Control
KOZ	Keep-Out-Zone
LEO	Low Earth Orbit
LiDAR	Light Detection and Ranging
LOS	Line Of Sight
MC	Monte Carlo
MPC	Model Predictive Control
R-GNC	Relative Guidance Navigation and Control
ROE	Relative Orbital Elements
RPO	Rendezvous and Proximity Operations
RTN	Radial Tangential Normal frame
STM	State Transition Matrix
WSE	Walking Safety Ellipse

1. Introduction

In the last few years, the launch activities in Low Earth Orbit (LEO) have dramatically changed the space economy. Particularly, the implementation and deployment of large constellations for providing broadband global internet coverage from orbit have rapidly overcome any other launch activities in LEO [1]. In this growing "ecosystem", the issue of sustainability of the space environment needs to be addressed and

should involve solutions to guarantee the long-term feasibility of such exploitation of space and orbit resources.

Considering this large number of satellites in orbit, the probability of contingencies and failures of some of the constellation's assets become important and will affect the congested orbital region of operations of the constellations. Several studies have pointed out how the LEO debris environment in presence of limited post mission disposal success rate of the large constellation assets could affect the debris population in the future. In Virgili et al. [2], the effect of post mission disposal success rate to the sustainability of the space environment is shown using four different models for simulating the debris population evolution over 200 years. Radke et al. [3] have shown that for the case study of the OneWeb constellation (first generation) there is a 35% of probability of creating fragments in orbit during the constellation mission lifetime and studied the long-term effect of the fragments cloud in the constellation orbital slots. Also, in [4] and [5] the effects of constellation traffic in the LEO environment evaluating the debris evolution in function of the post mission disposal success rate and estimating the future number of collisions. Moreover, the increase of the collision risks in the constellations' orbital region will impact the collision avoidance warnings and manoeuvres for the operational assets during their lifetime.

To mitigate these effects, an Active Debris Removal (ADR) service is discussed in this work. Several efforts in the last few years have been dedicated to studies and design of active debris removal missions [5][7][8]. The development of commercial ADR service for large constellations assets has been recently discussed as a business case to pave the way to the debris removal and in orbit servicing activities which will change the paradigm of space resource exploitation. The ADR service mission design to multiple constellation targets has been studied in the last few years [9][10][11]. The focus of this work is the Rendezvous and Proximity Operations (RPOs) required during the ADR service mission to approach, capture and deorbit the debris object. The work of this paper is part of the phase A design of the ADR service under the ESA/OneWeb funded Sunrise programme. The effort was taken by a consortium led by D-Orbit S.p.a. with the collaboration of Politecnico di Milano.

The paper is organised with a first brief description of the mission concept considered for the service mission under study and the proximity operations required within the mission. Subsequently, the Concept of Operations (ConOps) in proximity is designed, together with the ADR payload required onboard the servicer. Then, the paper will dive in the core of the proximity operations design, presenting the analysis and solutions for the phases prior capture. Finally, the conclusions and next steps are discussed providing the proximity operations delta-v budget for the ADR service.

2. Service mission concept overview

The mission concepts for the active removal of failed constellations satellites have been considering a multiple target's mission. In [9][10], different mission architectures are considered for the ADR service. The mission architectures discussed foresee a rigid capture mechanism to capture the target, such as a robotic arm, thanks to high TRL of the technology in space.

In the following a brief description is provided with the aim of introducing the proximity operations required for the mission architectures studied. The first mission architecture is the chaser mission, where the servicer is designed to approach sequentially each failed satellite in a constellation, capture the satellite and transfer it in a disposal orbit complaint with a five year re-entry time. Then the servicer will move on to the next constellation target. Another explored mission concept is the mothership architecture, where the servicer approaches each failed asset of the constellations and attaches deorbiting kits to the target's platform which then will independently perform the deorbiting. In this architecture the delta-v used for the transfer from and to the disposal orbit after each target is saved. Subsequently, the chaser plus station mission architecture is considered where one servicer is used to capture and deorbit each target, but a station for refuelling is considered to replenish the chaser during the service.

The trade-off of the mission architecture, mostly in terms of costs identify different mission architectures as the optimal one. Nonetheless, the main challenges and functions that the servicer shall perform in the proximity of the target remain similar prior the capture to the target. One difference is that for the mothership architecture, the capture and installation of deorbiting kit requires additional requirements and operations after capture. Nonetheless, the main challenges in the proximity operations prior capture are then the approach to the uncooperative failed satellite and the preparation of the conditions for rigid capture. In the station + chaser architecture, also the rendezvous and docking with the station will take place, but it will have a cooperative and collaborative nature which will present less challenges with respect to the uncooperative case.

3. Proximity concept of operations

The focus of this work is on the design of the RPOs to the uncooperative object, including the operations prior the robotic capture of the debris. The ConOps of the approach to the uncooperative and non-collaborative

target is discussed in this section. In this study two different baseline constellation targets are considered, with the characteristics shown in Table 1. The targets are selected as representative targets of the constellation population, including small class satellite (light target) and large class satellite (heavy target). The main high-level requirements in the definition of the proximity ConOps and in the approach strategies are:

- **Req-1:** The servicer shall be able to rendezvous and capture the target. No cooperation nor collaboration from the target shall be considered.
- **Req-2:** The servicer shall be equipped with onboard sensors dedicated to the measurement of bearing, range and pose of the target to enable and support the rendezvous operations.
- **Req-3:** The servicer shall be able to capable to perform the final operations in proximity regardless of the natural illumination conditions.

Table 1. Constellation satellites taken as baseline in the ADR service design.

	Light Target (LT)	**Heavy Target (HT)**
Reference platform	OneWeb Arrow spacecraft	EliTeBus-1000 bus (GLOBALSTAR and Iridium-NEXT)
Mass [kg]	150	750
Altitude [km]	1200	1420
Inclination [deg]	87.9	52

Two of the most important high-level drivers in the design of an ADR service for large constellation is the need of autonomy and safety, which will benefit the mission cost and operations. In addition, being the servicing mission cost and benefit strongly related to the number of targets deorbited and/or serviced within the same mission, the success each of the servicing shall be ensured before moving to the next target of the mission.

The proximity ConOps envisioned is shown in Fig. 1. The sequence of operations in chronological order during the mission timeline of one service to a failed constellation asset are the following:

1. Absolute orbit phasing
2. Far-range rendezvous
3. Mid-range rendezvous
4. Inspection
5. Target preparation for robotic capture
6. Final approach forced motion
7. Robotic operations and capture
8. Stack stabilisation and deorbiting

After a coarse orbit phasing managed by the absolute Attitude and Orbit Control System (AOCS) of the servicer, the proximity operations will start at the activation of the on-board relative sensors as soon as the target can be detected with the onboard relative sensors. The designed mean separation in the along-track direction for the proximity operations start is considered around 50 km. During the far-range rendezvous, the servicer will reduce the mean along-track separation with the target with impulsive manoeuvres to reach distances of about 1 km in separation in the along-track direction using a spiralling trajectory ensuring passive safety. In the far-range rendezvous phase, the servicer is required to maintain a pointing attitude guidance at the along track direction towards the target. The mid-range rendezvous will then continue the reduction of the along-track separation to few hundred meters. Differently from the far-range rendezvous, in the mid-range the servicer attitude guidance might require a synchronisation with the relative dynamics during the spiralling trajectory to keep the target in the relative sensors Field of View (FOV). Additionally, in the mid-range the range measurement with a dedicated sensor will complement the Line of Sight (LOS) measurement to aid the navigation solution. Subsequently, from few hundred meters of separation to the target, the inspection phase will begin with the aim of activation and verification of the close-range sensors and acquisition of the target physical and dynamical states knowledge. The trajectory guidance is here designed considering a walking safety ellipses sequence around the target accounting for illumination conditions on the orbit. After a reliable pose estimation of the target is acquired in the inspection phase, the servicer will decide whether to proceed with the close-range terminal approach to the capture hold point or performing additional operations to allow the mission advancement. In fact, in cases where the tumbling state of the failed satellite is greater than the designed threshold, the servicer is considered not capable to autonomously approach the capture hold point with a forced motion profile. In such cases, an additional phase of target preparation for rigid capture is envisioned, where the target angular rate is damped using a contactless control with plume impingement with the servicer's thrusters.

Once the target is in a condition to be captured, the forced motion synchronisation profile is performed to bring the servicer to the capture hold point and perform the robotic capture operations. After the securing of the capture, the servicer will deorbit the target by transferring the stack to the disposal orbit.

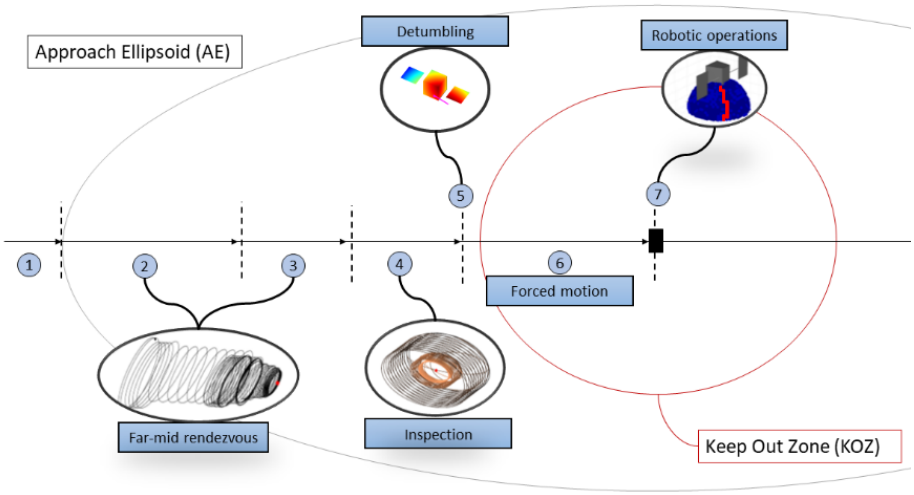

Fig. 1. RPOs Concept of operations for each service to a failed uncooperative satellite of the constellation fleet.

To achieve a successful completion of the whole proximity operations, a set of payloads specifically dedicated to the ADR functions in proximity must be embarked on the servicer platform. Particularly, the set of relative sensors reported in Table 2 have been preliminary designed after a trade-off in the technological options.

Table 2. ADR sensors payloads employed for the proximity operations.

Sensor	***Range [km]***	***FOV range [deg]***	***Mass [kg]***	***Power [W]***
VIS NFOV camera	50 - close	6 - 12	~1	~10
VIS WFOV camera	10 - close	40 – 60	~1	~10
IR camera	3 - close	12 - 40	~1	~10
Flash Lidar	3 - close	15 - 30	~5	~50

In the far-range phase, the main sensor used is the Narrow Field Of View (NFOV) Visible Camera, which is capable of providing bearing information of the servicer-target formation. This will allow the angles-only navigation solution to estimate the target state. An additional camera with Wide Field Of View (WFOV) in the Visible part of the spectrum is used to provide image measurement from closer range to the target keeping the whole target body in the FOV. The visible camera has the advantage of being a space proven technology which have flown in a variety of missions; however, the measurement acquisition will be sensitive to the in-orbit illumination conditions of the target. The baseline target constellation considered in LEO, reported in Table 1, will experience eclipse conditions and a wide variety of target illumination conditions depending on the right ascension of the ascending node and the Sun position at the time of service. Therefore, to improve robustness to illumination conditions an infrared sensor is considered to work in closer range to provide image measurements of the target in the cases of poor illumination. The operational range of the infrared sensors is considered of 1-3 km of maximum operational range, to guarantee continuous measurement in poor illumination conditions at closer range, where the divergence of the filters from lack of measurement will strongly affect the safety of the rendezvous. Additionally, the infrared sensor mass will be limited if the operational range is limited, requiring a smaller sensor. At last, a Flash Imaging and Detection (LiDAR) sensor is envisioned on board the satellite to provide the range measurements of the target from mid-range, otherwise not achievable with passive sensors other than the coarse measurement coming from the passive 2D image acquired highly sensitive to the target condition and illuminations conditions. The LiDAR is considered with the flash imaging technology, which has less accuracy but lower mass and system complexity of the scanning system counterpart. The flash imaging LiDAR is considered working from operational ranges of approximately 3 km up to the close range where it will provide the 3D point map of the target to complement the pose estimation solution.

The sensors operation matrix of the proximity operations is shown in Fig. 2, where the superposition of the operational range and measurement provided between sensors is specifically designed to include the redundancy of the sensor assembly and increase the robustness of the navigation solution.

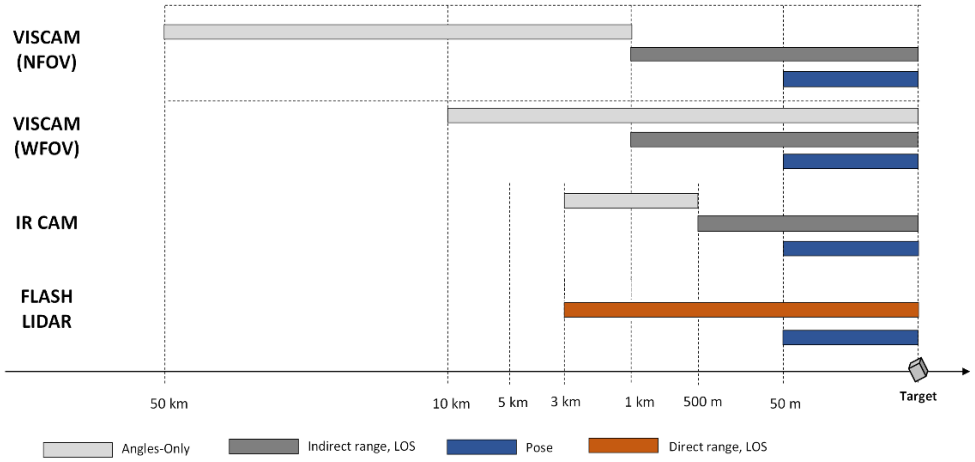

Fig. 2. Operations matrix of the sensor suite in function of the separation distance during the proximity operations.

4. Far and mid-range rendezvous design

In this section, the strategies adopted to design the far and mid-range rendezvous GNC are described. Each subfunction of the Relative Guidance Navigation and Control (R-GNC) block of the servicer is presented and the simulations results in a high-fidelity environment are discussed. In this initial phase of the proximity operations the servicer is required to reduce the separation distance with the target to reach closer proximity in a safe and autonomous fashion.

4.1 Relative Guidance and Control approach

The guidance and control solution are based on the framework originally introduced by Gaias et al. [12][13], which used impulsive manoeuvres to control the relative motion between two satellites. The general idea of this framework is to decouple the Guidance and Control (GC) solutions with the aim of obtaining a computationally efficient algorithm. Particularly, the GC solutions will be obtained in an analytic fashion which will greatly benefit the onboard autonomous implementation of the routines. The relative motion dynamics in circular orbits parametrised in Relative Orbital Elements (ROE) and forced with n impulsive manoeuvres at time t_i can be expressed as follows:

$$a\delta\boldsymbol{\alpha_f} = \Phi_{0,f}\, a\delta\boldsymbol{\alpha_0} + \Phi_{1,f} B_1 \delta\boldsymbol{v_1} + \cdots + \Phi_{n,f} B_n \delta\boldsymbol{v_n} \quad (1)$$

Where $\Phi_{i,j}$ is the State Transition Matrix (STM) from time t_i to time t_j , B_i is the control input matrix obtained from the Gauss Variational Equations (GVE) [14]. The ROE state vector $a\delta\boldsymbol{\alpha}$ is defined as follows [14]:

$$a\delta\boldsymbol{\alpha} = \begin{bmatrix} \delta a \\ \delta\lambda \\ \delta e_x \\ \delta e_y \\ \delta i_x \\ \delta i_y \end{bmatrix} = \begin{bmatrix} (a - a_d)/a_d \\ u - u_d + (\Omega - \Omega_d)\cos i_d \\ e\cos\omega - e_d\cos\omega_d \\ e\cos\omega - e_d\cos\omega_d \\ i - i_d \\ (\Omega - \Omega_d)\sin i_d \end{bmatrix} \quad (2)$$

In this work, the STM used include the mean J_2 effect on the relative motion dynamics. The drag effects are neglected due to the limited influence on the motion at the high altitude of the constellations taken as a baseline in Table 1.

The adopted solution exploits the knowledge of the relative dynamics' evolution in the ROE space, and instead for solving directly for the $\delta\boldsymbol{v_i}$ to reach the desired condition will shape the trajectory in the ROE space. To this aim, the guidance is expressed in the ROE space in function of the forced ROE jumps $a\Delta\delta\alpha_i$ as follows:

$$a\delta\alpha_f = \Phi_{0,f}\, a\delta\alpha_0 + \Phi_{1,f}\, a\Delta\delta\alpha_1 + \cdots + \Phi_{m,f}\, a\Delta\delta\alpha_m \quad (3)$$

Then the guidance is produced computing the required ROE jumps to achieve the final desired condition and satisfying the minimisation of a cost function. As cost function in this paper a modification of the one in [12] is adopted, which is composed by two main terms:

$$J = J_e + w\, J_o \quad (4)$$

The first term is related to the quadratic cost function of the distance spanned in the ROE space by the ROE jumps and is expressed as follows:

$$J_e = \sum_i^m \|a\Delta\delta a\|^2 + \sum_i^m \|a\Delta\delta\lambda\|^2 + \sum_i^m \|a\Delta\delta\boldsymbol{e}\|^2 + \sum_i^m \|a\Delta\delta\boldsymbol{i}\|^2 \quad (5)$$

Where $a\Delta\delta\boldsymbol{e}$ and $a\Delta\delta\boldsymbol{i}$ represent the norm of the eccentricity and inclination vector jumps respectively. Such definition of the cost function represents the 6D distance spanned by the manoeuvres in the ROE space and is directly related to the energy involved in the forced transfer, i.e., delta-v needed for the trajectory implementation. Considering Equation (5), and expressing the final ROE jump in function of the previous one enforcing the final state constraints, the equation can be written in function of the $m-1$ ROE jumps along a trajectory. Moreover, denoting as $\boldsymbol{x}_i$ as the *i*-th ROE jump vector the cost function can be written as follows:

$$J_e = \boldsymbol{X}^T\boldsymbol{X} + (D + H\boldsymbol{X})^T(D + H\boldsymbol{X}) \quad (6)$$

With

$$D = \Phi_{m,f}^{-1}[a\delta\alpha_f - \Phi_{0,f}a\delta\alpha_0] \quad (7)$$

$$H = -\Phi_{m,f}^{-1}\,[\Phi_{1,f} \quad \Phi_{2,f} \quad \dots \quad \Phi_{m-1,f}] \quad (8)$$

Where $X = [x_1, x_2, \dots, x_{m-1}]^T$ denotes the rearrangement of the ROE jumps vectors. It can be readily noted how the cost function assumes a simple quadratic form in function of X.

The second term J_o in Equation (4) serves as an index of observability of the guidance trajectory, weighted by a constant term w. In fact, as it will be explained in detail in the next sub-section, to approach the target from large separation the servicer will exploit the Angles-Only (AO) navigation strategy. In the natural relative dynamics, the AO strategy is inherently not fully observable. The performance index introduced in this work aims at reducing this drawback at the guidance level. In literature, several observability definitions for the angles-only problem can be found, particularly in presence of manoeuvres [15][16][18]. In practice, the full observability of the relative state is retained after an impulsive manoeuvre. However, different manoeuvres will induce different LOS variations, introducing a what is here called degree of observability. In presence of sensors errors, the degree of observability introduced by each manoeuvre is crucial to the subsequent improvement of the navigation solution. Exploiting the definition of [15], the observability condition can be expressed as:

$$(\delta x^N(t_1))^T(\delta x^M(t_1)) = 0 \quad (9)$$

Where $\delta x^M(t_1)$ represent the position vector of target at time $t_1 > t_0$ after an impulsive manoeuvre at time t_0, while $\delta x^N(t_1)$is the position vector at time t_1 only due to the natural dynamic evolution without the influence of the manoeuvres. In an intuitive way, the degree of observability is defined using Equation (9), which represents the distance of the two vectors at time t_i. Including this property at guidance level requires the transformation of the condition into the ROE space. The condition of Equation (9) can be enforced in *K* observability nodes at times t_k, comparing the states at node *k* and *k-1*:

$$\left(\Gamma(t_k)\delta\alpha_k^N\right)^T\left(\Gamma(t_k)\delta\alpha_k^M\right) = 0 \quad (10)$$

The matrix $\Gamma(t_k)$ represents the mapping between the cartesian relative state vector with the ROE vector at time t_k. The observability enhancement at node t_k is then obtained minimising this expression in function of the ROE states along the guidance trajectory. The choice of each observability nodes must be taken with care considering the eclipsing conditions and Sun position. The performance index to be included in the guidance cost function is then the cumulative contribution of each observability node defined.

$$J_o = \sum_k^K \left(\Gamma(t_k)\delta\alpha_k^N\right)^T\left(\Gamma(t_k)\delta\alpha_k^M\right) \quad (11)$$

Manipulating the expression of Equation (11), and considering the observability nodes coincident with the guidance nodes $t_i = t_k$, the observability cost function can be expressed in function of the *m-1* guidance ROE jumps:

$$J_o = \sum_i^K X^T O_{1,i} + X^T O_{2,i} X \quad (12)$$

Finally, the expression of Equation (12) is a quadratic function in the ROE jump states *X*. The selection of the ROE jumps *X* to minimise the *J* function is then obtained computing the stationary point of the first variation of *J* with respect to *X* as follows:

$$\frac{\partial J}{\partial \boldsymbol{X}} = (G_2)X + \bar{D} = 0 \quad (13)$$

With

$$G_2 = I + H^T H + w\sum_k^K O_{2,j} \quad (14)$$

$$\bar{D} = I + H^T H + w \sum_{k}^{K} O_{2,j} \quad (15)$$

The solution of the linear system in Equation (13), provides then the delta-v sub-optimal guidance solution in the ROE space.

Then, once the guidance trajectory is computed, the control actions to obtain the *X* sequence of ROE forced variations are computed through the analytic optimal schemes described in [17]. The reconfiguration problem between $\delta\alpha_i$ and $\delta\alpha_{i-1}$, with j impulsive manoeuvres, can be expressed as:

$$[\Phi_{i,1}B_1 \quad \Phi_{i,j}B_j]\begin{bmatrix}\delta v_1 \\ \dots \\ \delta v_j\end{bmatrix} = \left(\delta\boldsymbol{\alpha_i} - \Phi_{i-1,i}\delta\boldsymbol{\alpha_{i-1}}\right) = \boldsymbol{x_i} \quad (16)$$

The scheme adopted considers the in-plane and out-of-plane problem decoupled from one another. Particularly, the in-plane reconfiguration problem is solved using three tangential manoeuvres placed at the argument of latitudes defined as:

$$u_j = \text{atan}\left(\frac{\Delta\delta e_y}{\Delta\delta e_x}\right) + k_j\,\pi \quad (17)$$

Regarding the out of plane impulsive control reconfiguration problem, one normal manoeuvre is performed at argument of latitude computed as:

$$u_j = \text{atan}\left(\frac{\Delta\delta i_y}{\Delta\delta i_x}\right) \quad (18)$$

More details on the control scheme optimality and assumptions can be found in [17].

4.2 Relative navigation approach

Along the far and mid range approach, the servicer shall be able to estimate the target relative state using an onboard navigation routine. From far range, the use of a visible camera providing bearing only measurements restricts the adoption of an angles-only navigation strategy acquiring bearing measurements of the target with the servicer onboard sensors, characterised by well-known observability issues.

The onboard real-time navigation is then performed using an Extended Kalman Filter (EKF), based on the estimation of the relative orbital elements state. The state transition model of the filter is based on the state transition matrix solution of the J_2 perturbed dynamics. On the other hand, as explained in Sect. 3, the servicer ADR payload design foresees the use of a LiDAR system capable of providing range measurements from around 1-3 km. The navigation solution in mid-range, thus the filter convergence, is then enormously aided by the full observability conditions provided by adding a range information with the LiDAR sensor. The sensors and EKF filter parameters selected for this preliminary analysis and simulations are reported in Table 3.

Table 3. Sensors' parameters used for the navigation in the simulations.

Sensor	*Parameter*	*Value*
Visible Camera	Noise	80 arcsec
	Measurement rate	0.1 Hz
LiDAR	Noise	50 cm
	Measurement rate	0.0015 Hz

The relatively low updates rates for the measurements acquisitions are defined considering at this design stage the constraints of different in-orbit operations of the service platform during the approach, together with limiting LiDAR power consumption.

4.3 R-GNC architecture and simulation results

The GNC during the far and mid-range approach is implemented considering a shrinking horizon Model Predictive Control (MPC), where at each GNC update, the guidance and control solutions are updated according to the filter estimate. This solution allows the update of the GC solution as the navigation solution improves, reducing the errors induced by the open-loop computed trajectory. The preliminary simulation campaign to validate the approach GNC system is performed considering the phases shown in Table 4.

Table 4. Far and mid-range rendezvous phases considered in the simulations, together with the R-GNC mode used.

Phases	**Guidance and control**	**Navigation**	**Separation**
Far-range 1	Observability enhanced (w)	AO	From 50 km to 10 km
Far-range 2	Energy optimal	AO	From 10 km to 1 km
Mid-range	Energy optimal	A + range	From 1 km to 500 m

The performances are evaluated simulating the GNC subsystem in a high-fidelity environment. The drag effects have been neglected at first iteration in the simulations due to the high altitude of the orbits considered.

At the first phase in far-range, the observability enhancement strategy is employed considering only the first observability node. For each case considered, with

different the observability cost function weight *w*, 100 Monte-Carlo simulations have been performed. Table 5 shows the mean values of the errors for each case considered. It can be appreciated, increasing the observability weight *w* the final errors in control and the final error in the relative longitude estimate decrease at the expense of a more demanding GC solution in terms of delta-v cost. In Fig. 3, the ROE time histories during the far-range 1 phase for a GNC solution with $w = 0.015$ is shown, together with the real-time onboard filter estimate. While Fig. 4 shows the time history of the filter estimate $a\delta\hat{\alpha}$ error with respect to the true relative state in the same simulation case.

Table 5. Results of simulations for different cases of w. The reported values represent the mean values over the 100 MC runs of the GNC.

	Navigation errors	**Control errors**	
w [-]	$a\delta\lambda_f - a\delta\hat{\lambda}_f$ [m]	$a\delta\lambda_f - a\delta\lambda_{f-d}$ [m]	δv_{tot} [m/s]
0	778.4	1989.1	6.05
0.005	652.3	1874.7	6.24
0.010	506.5	1509.3	6.76
0.015	399.7	1125.6	7.48
0.020	349.9	897.9	8.33
0.025	303.9	732.5	9.14
0.030	263.5	567.8	9.93
0.035	229.8	465.8	10.87

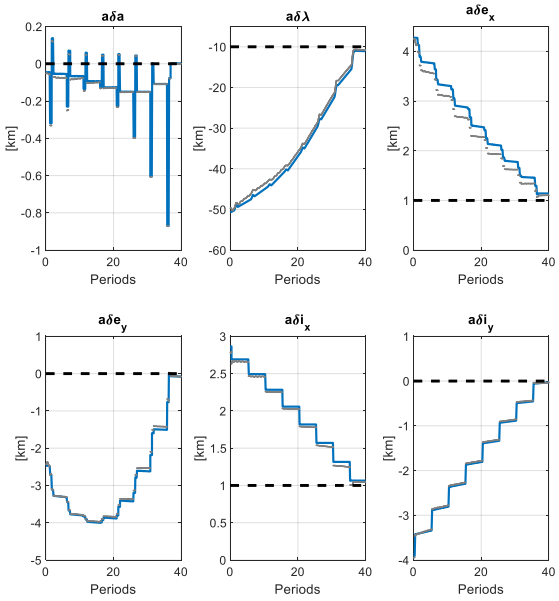

Fig. 3. ROE time histories for the far-range 1 phase, considering w = 0.001. In blue the real ROE state time history is shown, while in light gray the onboard navigation filter estimate.

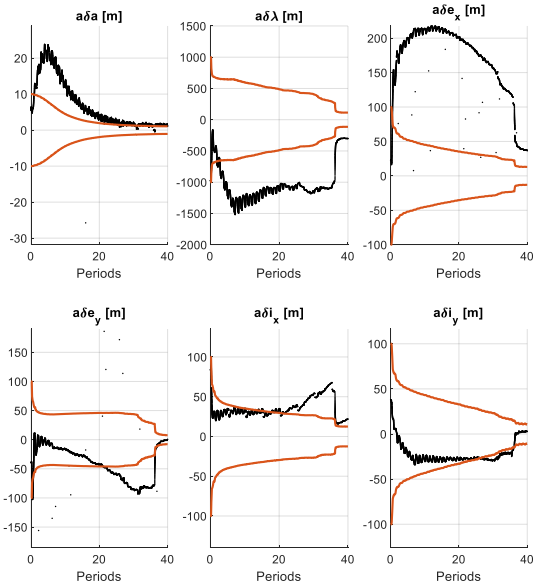

Fig. 4. Navigation estimate errors during the far-range 1 phase (black). Error envelopes (orange) are derived from the diagonal components of the filter covariance matrix output.

The observability enhancement feature affects the geometry of the relative approach, as shown in Fig. 5 and Fig. 6. It can be noted, from the plots of the trajectory in the RN plane how the increase of observability sought in the first phase $\boldsymbol{x_1}$ influences the shapes of the trajectory in RN, achieving a higher difference in LOS at the first node. From Fig. 5 and Fig. 6, it can be noted that the feature of passive safety intended as E/I separation during the approach is well respected. In this design, the E/I separation is checked after the computation of the GC solution, without directly including the E/I separation constraints at guidance level. However, these counter measures have been considered to guarantee E/I separation of the rendezvous approach:

- Definition of target state of far-range 1 characterised by parallel (or anti-parallel) relative eccentricity and inclination vectors. In this way, the trajectory over the whole approach is forced to meet the E/I perfect separation before reducing further the separation towards the target.
- Limiting the magnitude of the ROE jumps required by the guidance scheme, by considering enough configuration nodes at guidance level to limit and an appropriately long configuration final time $\boldsymbol{t_f}$.

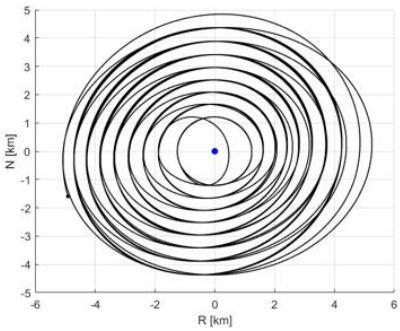

Fig. 5. Far-range 1 phase trajectory in the RN plane with no observability enhancement (w=0).

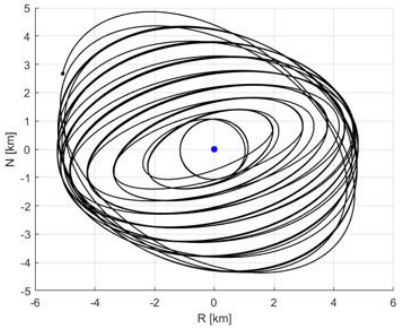

Fig. 6. Far-range 1 phase trajectory in the RN plane with observability enhancement (w=0.015).

Concerning the far-range 2 and mid-range simulations, the results for 100 Monte-Carlo (MC) simulations of each phase are shown in Table 6. Fig. 7 demonstrates the improvement of the navigation solution in the mid-range phase, thanks to the LiDAR range measurements taken at 0.0015 Hz (approximately 10 times per revolution).

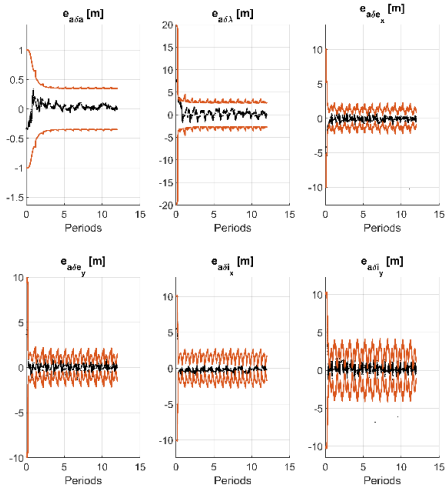

Fig. 7. Navigation estimate errors during the mid-range phase (black). Error envelopes (orange) are derived from the diagonal components of the filter covariance matrix output.

Table 6. Far-range 2 and mid-range approach results. The results reported refers to the mean values out of the 100 MC simulations performed.

	Navigation errors	**Control errors**	
	$\hat{\boldsymbol{e}}_{\boldsymbol{\delta\lambda}}$ [m]	$\boldsymbol{e}_{\boldsymbol{\delta\lambda}}$ [m]	$\boldsymbol{\delta v_{tot}}$ [m/s]
Far-range 2	14.14	10.95	0.83
Mid-range	0.03	3.59	0.50

5. Inspection

After the reduction of the servicer-target separation up to few hundred meters with the R-GNC functions at the end of mid-range approach, the servicer has acquired a reliable estimate and knowledge of the translational state of the target. However, to proceed with the close-proximity operations, a dedicated inspection phase in required. In this phase, the servicer performs a series of manoeuvres and fly-arounds which allows the on-board observation of the target pose and physical characteristics. A reliable knowledge of aforementioned information is a strict requirement to receive the go-command from ground and proceed with the closer approach forced motion and operations. The relative sensors employed in this phase comprehend the passive cameras suite and the flash LiDAR sensor.

In the inspection phase, the trajectories are designed to exploit the natural relative dynamics to obtain the required fly-around the target body. The strategy adopted consist in the use of Walking Safety Ellipse (WSE) to fly around the envelope around the target in the RTN frame. These peculiar trajectories can be defined in the ROE space, considering a E/I separation and a residual semimajor axis difference δa. Such design results in drifting spiralling trajectory around the target, with a guarantee minimum safe separation in the RN plane.

The preliminary designed considered here, reported in Table 7, include three different spirals geometries characterised by different magnitudes of the relative eccentricity and inclination vector, controlling the RN separation over the drift trajectory. The relative semimajor axis of each of the orbits is obtained considering the drift from a symmetric condition at the other side of the target in a fixed time (taken here equal to 8 orbital periods). The plus and minus in Table 7 refers to the walking safety ellipses drifting from negative to positive values of relative argument of longitude $\delta\lambda$ and vice versa respectively. The keep-out zone in the design presented in this paper is considered is defined relative to the LT OneWeb platform, and is equal to 16 m. In the case of the HT platform, the keep-out zone of 36 m will influence the parameters designed for the WSE of Table 7 to guarantee a larger RN distance.

Table 7. WSE parameters selected for the inspection sequence of the LT (OneWeb platform).

	$\|a\delta\boldsymbol{e}\| = \|a\delta\boldsymbol{i}\|$ [m]	$\psi = \theta$ [deg]	$a\delta a$ [m]	$a\delta\lambda$ [m]
WSE1 +	150	0	-12.7	-600
WSE1 -	150	90	12.7	600
WSE2 +	75	90	-6.3	-300
WSE2 -	75	180	6.3	300
WSE3 +	50	180	-6.3	-300
WSE3 -	50	270	6.3	300

In the design of the forward (+) and backward (-) drifting WSE, the relative eccentricity vector and inclination phasing has is changed of +90 deg. This design is developed considering eclipse regions and target illumination conditions. To evaluate the illumination conditions of the target, the angle γ between the Sun vector in RTN and the servicer-target position vector is evaluated. Assuming that the servicer points the sensor towards the target, when the angle γ is lower than 130 deg, the target is considered in a well-suited illumination condition for observation. Due to the motion of the Sun vector in the rotating RTN frame, the change of relative phasing of the relative eccentricity and inclination vector will influence the phasing with the Sun vector motion. The induce relative phasing change of 90 deg allows the blind regions to cover different spiral regions in RTN. The trajectories shown in Fig. 8 show the effect of the change in the eccentricity and inclination vector phasing, displaying in magenta the blind regions of the WSE. In the design, due to the limited duration of one WSE sequence (plus and minus), the Sun vector in the inertial frame is considered stationary, simplifying the modelling of its motion in the RTN frame. To transfer from one WSE to the other, the strategy of impulsive manoeuvres is used described in Sect. 4.1. In this case, however, the out-of-plane manoeuvre is split into three manoeuvres performed in correspondence of the tangential manoeuvres u. In such a way, for the reconfiguration problems defined by the inspection sequence, the E/I separation is guaranteed also during the manoeuvre sequence other than during the WSE drift. The delta-v spent for each reconfiguration within the inspection sequence is reported in Table 8.

Table 8. delta-v spent in the reconfiguration transfers in the inspection sequence for the light target.

Transfer	$\|\boldsymbol{\delta v}\|$ ***[m/s]***
WSE1+ → WSE1-	0.304
WSE1- →WSE2-	0.135
WSE2- →WSE2+	0.152
WSE2+ →WSE3-	0.039
WSE3- →WSE3+	0.101
Total	**0.733**

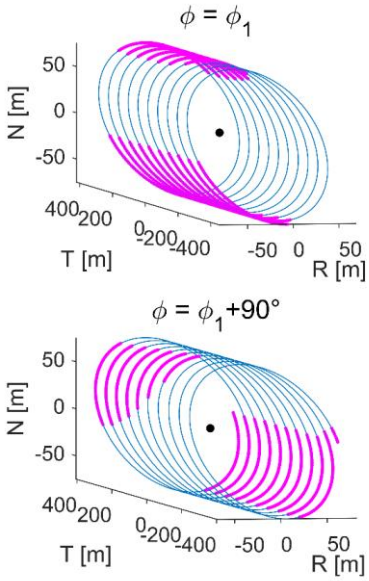

Fig. 8. WSE2+ trajectory (top), WSE2- trajectory in the RTN frame. Magenta regions represent the eclipse plus poor illumination conditions.

6. Rigid capture preparation operations

After the inspection phase is finished, the servicer has acquired reliable measurement and information on the target dynamic and physical state. The next operations will then depend on the target tumbling state. In fact, a rigid capture with a robotic arm of a tumbling satellite will present several problems in the operations and systems:

- Safety conditions in the approach and manipulator operations in the case of fast rotating target.
- The synchronisation accelerations profile required by the chaser to reduce the relative motion of the approach direction of the target in the servicer body frame. In the case of fast tumbling object, it may be unfeasible for the servicer systems.
- Robotic arm requirements in terms of maximum torque and power during the stabilisation phase after capture has been secured.

To perform the rigid capture, the relative motion of the target capture point in the servicer body frame needs to be limited. For the two constellations targets taken as a baseline, different capture points have been preliminary identified. For the light target, shown in Fig. 9, the capture point is identified correspondent to a dedicated grapple fixture located in the positive X_B face of the target's body frame. On the other hand, the heavy target capture point is identified in the positive Z_B of the body frame, shown in Fig. 10, correspondent to the launcher

adapter structure. To fully synchronise with the target capture direction motion, the servicer shall be able to compensate the centrifugal accelerations to keep itself approximately stationary in the target body frame. In this framework, the threshold of 1 deg/s is considered as the limit for the safe synchronisation of the servicer with the approach direction after a study and trade-off on the acceleration level required for synchronising at different distances.

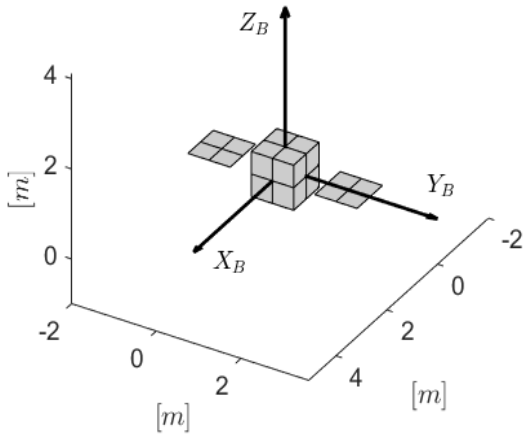

Fig. 9. Light target simplified geometry considered.

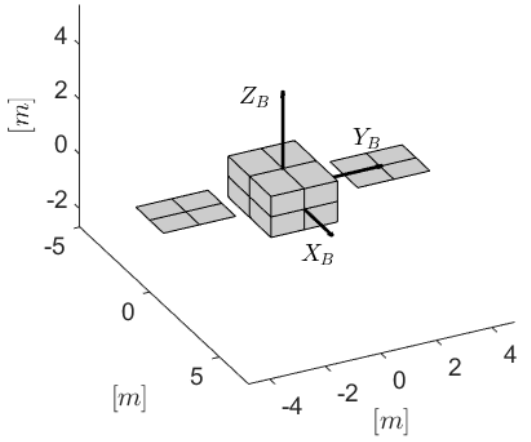

Fig. 10. Heavy target simplified geometry considered.

In the cases where the failed constellations satellite experiences a faster uncontrolled rotation, a dedicated phase in the ConOps is developed to prepare the target for the safe rigid capture operations. To this aim a strategy of contactless control of the target's tumbling state is used employing the plume impingement effects of the servicer's onboard thrusters [19][20]. The contactless strategy of plume impingement was selected thanks to the ability of providing control torques from a safe distance from the target, and the negligible impact on the system design of the servicer since it will employ the already available onboard thrusters.

For the impingement control operations, the servicer is assumed to be in a station-keeping position R at $+T$ outside the keep-out zone. The adopted strategy allows the impingement actions designed to produce torques on the target, to additionally contribute to the decrease of orbital energy of the target with forces in the -T direction. The control the servicer's thruster pointing to generate detumbling torques on the target is based on the algorithm explored in [20]. The main features of the algorithm are the onboard estimation of the plume impingement torque with an analytic pressure model of the thruster plume and the selection of the candidate pointing towards the target's body. The analytic plume model describes the pressure inside the plume as:

$$P(\theta, r) = C\, e^{\frac{\theta}{2\theta_0}} r^{-2} \tag{19}$$

Where θ is angle measured from the thruster centre line, r is the distance from the thruster nozzle exit. The half cone angle θ_0 represent the 1σ width of the plume, while the constant C is derived from the thrust F from continuity considerations. In the force modelling, the assumption of hyperthermal flow providing a diffuse reflection of the plume on the target's surfaces is considered.

$$d\boldsymbol{F} = -P(r,\theta)\cos\gamma\, dS \left[(1-c_s)\,\boldsymbol{S} + \boldsymbol{2}(c_s\cos\gamma + \frac{1}{3}c_d)\boldsymbol{N}\right] \tag{20}$$

The parameters used for the models and thrusters are reported in Table 9. The pointing guidance and the firing sequence are then based on the discrepancy between the estimated plume impingement torque with a detumbling guidance torque law:

$$T_g = -K\frac{\boldsymbol{h_L}}{\|\boldsymbol{h_L}\|} \tag{21}$$

Where $\boldsymbol{h_L}$ is the target rotational angular momentum vector expressed in the RTN frame.

Table 9. Impingement models parameters and KOZ distance considered in the control.

F [N]	θ_0 [deg]	c_s [-]	c_d [-]	R [m]	
10	12	0.03	0.97	LT: 16	HT: 36

Fig. 11, the results for simulation with different initial conditions show that initial tumbling motion of up to 11 deg/s can be managed by the plume impingement strategy. The higher initial tumbling rate will reflect in the longer stabilisation time needed and the greater delta-v cost of the impingement operations. Table 10 shows the results for the impingement detumbling strategy for the light and heavy constellations targets. The control for

three different tumbling motion regimes have been simulated. For each initial tumbling regime, 100 Monte Carlo simulations have been performed sampling the initial attitude state.

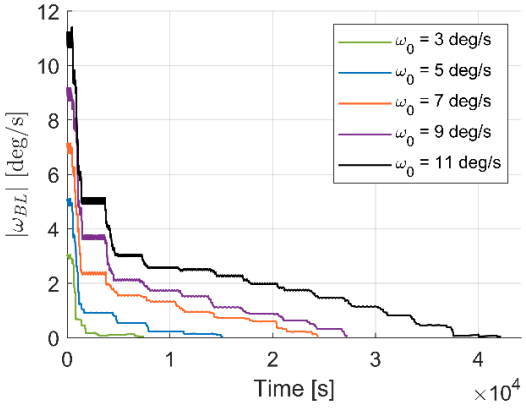

Fig. 11. Time histories of the angular rate of the target affected by the plume impingement control for different initial conditions.

Table 10: Impingement detumbling results for the light and heavy target.

		$\boldsymbol{\omega_0 = [\epsilon, \epsilon, 5]^T}$ **[deg/s]**	$\boldsymbol{\omega_0 = [\epsilon, 5, \epsilon]^T}$ **[deg/s]**	$\boldsymbol{\omega_0 = [5, \epsilon, \epsilon]^T}$ **[deg/s]**
Light target (LT)	$\overline{\delta v}$ [m/s]	4.61	14.47	5.60
	$max(\overline{\delta v})$ [m/s]	7.56	16.75	8.61
Heavy target (HT)	$\overline{\delta v}$ [m/s]	6.98	17.90	6.30
	$max(\overline{\delta v})$ [m/s]	13.39	19.75	8.31

7. Conclusions

In this work the phase A design of the proximity operations of an ADR service to large constellations failed satellite is described. Particularly, the phases of the far-range rendezvous, inspection sequence and rigid capture preparation have been described in detail including the feasibility study and the algorithms' design.

Acknowledgements

The research leading to these results has received funding from the European Research Council (ERC) under the European Union Horizon 2020 research and innovation program as part of the project COMPASS (Grant agreement No. 679086). www.compass.polimi.it.

References

[1] ESA Space Debris Office. (2021). ESA's Annual Space Environment Report.

[2] B. Bastida Virgili, J.C. Dolado, H.G. Lewis, J. Radtke, H. Krag, B. Revelin, C. Cazaux, C. Colombo, R. Crowther, M. Metz, Risk to space sustainability from large constellations of satellites, Acta Astronaut. 126 (2016) 154–162.

[3] J. Radtke, C. Kebschull, E. Stoll, Interactions of the space debris environment with mega constellations—Using the example of the OneWeb constellation, Acta Astronaut. 131 (2017) 55–68.

[4] Liou, J.-C., Matney, M., Vavrin A., Manis, A., and Gates, D., NASA ODPO's large constellation study, Orbital Debris Q. News, 22, (3), (2018) 4–7.

[5] H.G. Lewis, Evaluation of debris mitigation options for a large constellation, J. Sp. Saf. Eng. 7 (2020) 192–197.https://doi.org/10.1016/j.jsse.2020.06.007.

[6] R. Biesbroek, L. Innocenti, A. Wolahan, S.M. Serrano, e.Deorbit - ESA's Active Debris Removal Mission, in: Proc. 7th Eur. Conf. Sp. Debris, 2017.

[7] C. Blackerby, A. Okamoto, K. Fujimoto, N. Okada, J.L. Forshaw, J. Auburn, Elsa-D: an in-Orbit End-of-Life Demonstration Mission, in: Proc. Int. Astronaut. Congr. IAC, 2018.

[8] R. Biesbroek, S. Aziz, A. Wolahan, S. Cipolla, M. Richard-noca, the Clearspace-1 Mission: Esa and Clearspace Team Up To Remove Debris, in: Proc. 8th Eur. Conf. Sp. Debris, 2021: pp. 1–3.

[9] S. Huang, C. Colombo, J.L. Gonzalo, A. Masserini, M. Nugnes, L. Vallini, M. Petit, Preliminary mission analysis of active debris removal service for large constellations, Proc. Int. Astronaut. Congr. IAC, 2020.

[10] C. Colombo, S. Huang, G. Borelli, F. Cavenago, M. Nugnes, J.L. Gonzalo, G. Gaias, M. Massari, L. Vallini, M. Petit, P. Guerrieri, M. Valli, S. Antonetti, Mission Analysis and Design for an Active Debris Removal Service for Large Constellations, in: Proc. 8th Eur. Conf. Sp. Debris, Darmstadt, Germany, 2021.

[11] J. Forshaw, R. de Vos van Steenwijk, S. Wokes, S. Ainley, A. Bradford, J. Auburn, C. Blackerby, N. Okada, Preliminary design of an end-of-life ADR mission for large constellations, Proc. Int. Astronaut. Congr. IAC. 2019-Octob (2019) 21–25.

[12] G. Gaias, S. D', N.A. Amico, J.S. Ardaens, Generalised multi-impulsive manoeuvres for optimum spacecraft rendezvous in near-circular orbit, Int. J. Sp. Sci. Eng. 3 (2015) 68. https://doi.org/10.1504/ijspacese.2015.069361

[13] J.S. Ardaens, G. Gaias, Flight demonstration of spaceborne real-time angles-only navigation to a noncooperative target in low earth orbit, Acta Astronaut. 153 (2018) 367–382. https://doi.org/10.1016/j.actaastro.2018.01.044

[14] Simone D'Amico, Autonomous Formation Flying in Low Earth Orbit, 2010.

[15] J. Grzymisch, W. Fichter, Optimal Rendezvous Guidance with Enhanced Bearing-Only

Observability, J. Guid. Control. Dyn. 38 (2015). https://doi.org/10.2514/1.G000822

[16] G. Gaias, S. D'Amico, J.S. Ardaens, Angles-only navigation to a noncooperative satellite using relative orbital elements, J. Guid. Control. Dyn. 37 (2014) 439–451. https://doi.org/10.2514/1.61494

[17] G. Gaias, S. D'Amico, Impulsive maneuvers for formation reconfiguration using relative orbital elements, J. Guid. Control. Dyn. 31 (2015) 1036–1049. https://doi.org/10.2514/1.G000189

[18] J.S. Ardaens, G. Gaias, Angles-only relative orbit determination in low earth orbit, Adv. Sp. Res. 61 (2018) 2740–2760. https://doi.org/10.1016/j.asr.2018.03.016

[19] T. V. Peters, D. Escorial Olmos, COBRA contactless detumbling, CEAS Sp. J. 8 (2016) 143–165. https://doi.org/10.1007/s12567-016-0116-6

[20] G. Borelli, G. Gaias, C. Colombo, Rotational control with plume impingement to aid the rigid capture of an uncooperative failed satellite, 2020 AAS-AIAA Astrodyn. Spec. Conf. (2020) 1–20.